

A finite difference method for 3D incompressible flows in cylindrical coordinates

E. Barbosa, O. Daube^{*},

*Université d'Evry Val d'Essonne, Laboratoire de Mécanique et d'Energétique
d'Evry, 40 rue du Pelvoux CE 1455, 91020 Evry cedex, France*

Abstract

In this work, a finite difference method to solve the incompressible Navier–Stokes equations in cylindrical geometries is presented. It is based upon the use of *mimetic* discrete first order operators (divergence, gradient, curl), i.e. operators which satisfy in a discrete sense most of the usual properties of vector analysis in the continuum case. In particular the discrete divergence and gradient operators are negative adjoint with respect to suitable inner products. The axis $r = 0$ is dealt with within this framework and is therefore no longer considered as a singularity. Results concerning the stability with respect to 3D perturbations of steady axisymmetric flows in cylindrical cavities with one rotating lid, are presented.

Key words: Incompressible Swirling Flows - Navier-Stokes Equations - cylindrical coordinates - mimetic finite differences operators

Introduction

Incompressible flows in cylindrical configurations, i.e. in geometries exhibiting a symmetry around an axis, are of great interest for an impressive number of fluid mechanics problems, ranging from basic flows as Taylor Couette flows to industrial applications as flows in turbomachineries. However, the resolution of the Navier–Stokes equations in cylindrical coordinates involves some specific difficulties, especially when the computational domain contains the axis $r = 0$. In fact, because the equations contain terms in $1/r$, this axis is often referred as a coordinate singularity. Many attempts to overcome this

^{*} Corresponding author

Email addresses: barbosa@cemif.univ-evry.fr (E. Barbosa),
daube@cemif.univ-evry.fr (O. Daube).

difficulty appeared in the literature. Some authors chose to revert to cartesian coordinates in the vicinity of the axis but this approach seems to suffer from the drawback that non physical Fourier modes are introduced by the cartesian or general curvilinear grid as noted recently by Sotiropoulos and Ventikos [1] whose work uses a grid with a distorted structure, therefore promoting the separation of the sidewall flow. In most of the related literature, Fourier series are used in the azimuthal direction and the problem generally amounts to find *ad hoc* boundary conditions on the axis for each of the Fourier modes. In our opinion, this approach suffers from the fact that the radial and azimuthal velocity components are meaningless on the axis. This difficulty may be handled in the context of spectral collocation methods based for instance on Chebychev polynomials, by using the so-called Gauss-Radau points as collocation points [2,3]. A similar approach may be used in a finite difference context on a staggered grid and is found for instance in a more recent paper by Verzicco and Orlandi [4]. They designed a finite difference scheme using the radial momentum ru , the angular momentum rv and the axial velocity as unknowns, these quantities being defined at staggered locations. These choices allow them in particular, to assume a vanishing radial momentum on the axis, an assumption which is also used in the discretization of the diffusive term.

In this paper, we propose a finite difference scheme which is in many points similar to Verzicco's scheme, but which provides a rigorous treatment of the axis vicinity. For this purpose, discrete operators which mimic the usual properties of vector analysis as $\text{curl}(\text{grad}) = 0$ and $\text{div}(\text{curl}) = 0$, are used. In addition, the discrete divergence and gradient operators are negative adjoint with respect to the standard \mathbb{L}^2 inner products. This family of discrete operators, called mimetic finite difference operators, have been extensively studied by Hyman and Shashkov [5–7] in a general frame of logically rectangular grids. However, the present paper is restricted to the use of cylindrical coordinates which form an orthogonal system, a fact which greatly facilitates the analysis and the computations. According to [5], we first choose a staggered arrangement of the velocity components (i.e. the fluxes through the cell faces) on a regular grid. The mimetic finite difference operators are then rigorously derived from the discrete counterpart of Gauss theorem for the divergence and from the discrete counterpart of Stokes theorem for the vorticity. The discrete gradient operator is then formally defined as the negative adjoint of the discrete divergence with respect to suitable inner products. The main advantages of this approach are that it applies everywhere and that no additional approximation or assumption is required in the vicinity of the axis, though the discrete relations in these points may be different from the other locations. Along these lines, the key points are the definition of the divergence operator at the centers of the cells adjacent to the axis, and the definition of the axial component of the vorticity on the axis. The different second order operators which are needed in the course of the resolution are then defined by composition of two first order operators, therefore avoiding the appearance of a $1/r$

term at $r = 0$, and also allowing for a correct treatment of the coupling between the radial and azimuthal components of the velocity in the momentum equations. In addition, the non linear terms of the incompressible Navier–Stokes have been discretized in order that they do not contribute to energy production in the sense of the discrete inner product, therefore imitating the behavior of the non linear terms in the continuum case.

The validity of this approach was first checked for a 2D flow with a current crossing the axis and then for the now well known flow in a cylindrical container with a rotating lid. This latter flow has received a lot of attention in the last decade since it was considered by Escudier [8] as an example of vortex breakdown. Many numerical studies have been published [9–11], most of them being limited to axisymmetric flows. However, some 3D computations recently appeared in the literature [1,12,13,15,14] and will be compared to our results concerning the spatial nature, axisymmetric or 3D, of the first instability for different aspect ratios.

1 Governing Equations

Our goal was to design a numerical tool to study flows of incompressible fluid with kinematic viscosity ν , in a closed container possessing the SO(2) symmetry (see for instance figure (1)). Defining the Reynolds number Re as $Re = \Omega R_0^2 / \nu$ where R_0 is a reference length and Ω a characteristic rotation rate, the Navier–Stokes equations read:

$$\nabla \cdot \mathbf{v} = 0 \quad (1)$$

$$\frac{\partial \mathbf{v}}{\partial t} + (\mathbf{v} \cdot \nabla) \mathbf{v} = -\nabla p - \frac{1}{Re} \nabla \times \nabla \times \mathbf{v} \quad (2)$$

in which the diffusion terms have been written as the curl of the curl of the velocity. Concerning the time discretization, a second order time marching procedure is used which results in a time discrete system for the unknowns \mathbf{v}^{n+1} and p^{n+1} at each time step which may be written in the form:

$$(\sigma \mathbf{I} + \nabla \times \nabla) \mathbf{v}^{n+1} + \nabla p^{n+1} = \mathbf{S}^{n,n-1} \quad (3)$$

$$\nabla \cdot \mathbf{v}^{n+1} = 0 \quad (4)$$

The velocity–pressure coupling is handled by means of an incremental projection method [16]. Let us only recall that a provisional velocity \mathbf{v}^* is computed in a first step by solving an equation similar to the momentum equation (2)

and is then projected onto the space of divergence free vector fields by solving a Poisson equation with homogeneous Neumann boundary conditions:

$$-\nabla \cdot (\nabla \phi) = \nabla \cdot \tilde{\mathbf{v}}^* \quad (5)$$

$$\frac{\partial \phi}{\partial n} = 0 \quad \text{on the boundary} \quad (6)$$

The important point in the frame of this paper is that the second order differential operators that appear in both equations (2) and (5) may be written as compounds of first order differential operators, divergence, gradient and curl, a fact that will be exploited in the spatial discretization.

Remark: It is well known that these fractional step methods introduce an error on the tangential component of the velocity along the boundary, which is sometimes referred as a spurious numerical boundary layer. This point is not addressed here since it is not related to the choice of mimetic finite difference to perform the spatial discretization. Let us say that preliminary computations using an influence matrix technique for each Fourier mode did not show significant discrepancies at least for the considered range of Reynolds numbers.

2 The Discrete Spatial Operators

2.1 The staggered grid and associated discrete spaces

The computational domain is discretized by an uniform grid with increments $\Delta r = 1/M$, $\Delta \theta = 2\pi/N$ and $\Delta z = A/K$. Two kinds of cells are used as displayed on figures (2):

- (1) The regular cells: they correspond to $i \geq 1$ and are of parallelepipedic shape (figure (2)–a),
- (2) The axis cells: they correspond to $i = 0$ (figure (2)–b)

In figures (2) the staggered arrangement of the different variables is also shown:

- The velocity components are located at the centers of the cell faces normal to them,
- The vorticity components are located at the mid edges parallel to them,
- Scalar functions as pressure, divergence, or temperature, are located at the cell centers.

Our goal is to use discrete schemes preserving most of the operator properties of the continuum case. For this purpose, and along the lines of Hyman and Shashkov [5], mimetic finite difference operators are selected. They require

for a proper use, the definition of some discrete spaces and associated inner products.

- the space \mathcal{HS} of discrete vector fields $\underline{\mathbf{U}}$, with components defined at the centers of the cell faces normal to them, and with zero normal component on the boundary. Note that no components of $\underline{\mathbf{U}}$ are defined on the axis $r = 0$ and that the discrete velocity belongs to this space.

$$\mathcal{HS} = \left\{ \underline{\mathbf{U}} = (u_{i+1, j+\frac{1}{2}, k+\frac{1}{2}}, v_{i+\frac{1}{2}, j, k+\frac{1}{2}}, w_{i+\frac{1}{2}, j+\frac{1}{2}, k}) \right\}$$

\mathcal{HS} is equipped with the natural inner product (see [5]) which is obtained by a discrete quadrature by the trapezoidal rule of the integral definition in the continuous case.

$$\begin{aligned} (\underline{\mathbf{U}}, \underline{\mathbf{U}}')_{\mathcal{HS}} = & \sum_{i=0}^{M-1} \sum_{j=0}^{N-1} \sum_{k=0}^{K-1} \frac{\Delta r \Delta \theta \Delta z}{2} \\ & \left[r_{i+1} u_{i+1, j+\frac{1}{2}, k+\frac{1}{2}} u'_{i+1, j+\frac{1}{2}, k+\frac{1}{2}} + r_i u_{i, j+\frac{1}{2}, k+\frac{1}{2}} u'_{i, j+\frac{1}{2}, k+\frac{1}{2}} \right. \\ & + r_{i+\frac{1}{2}} (v_{i+\frac{1}{2}, j+1, k+\frac{1}{2}} v'_{i+\frac{1}{2}, j+1, k+\frac{1}{2}} + v_{i+\frac{1}{2}, j, k+\frac{1}{2}} v'_{i+\frac{1}{2}, j, k+\frac{1}{2}} \\ & \left. + w_{i+\frac{1}{2}, j+\frac{1}{2}, k+1} w'_{i+\frac{1}{2}, j+\frac{1}{2}, k+1} + w_{i+\frac{1}{2}, j+\frac{1}{2}, k} w'_{i+\frac{1}{2}, j+\frac{1}{2}, k}) \right] \quad (7) \end{aligned}$$

Where by convention $r_0 = 0$. For notation and programming convenience the quantity $u_{0, j+\frac{1}{2}, k+\frac{1}{2}}$ may be set to 0, despite the fact that it is normally not defined.

- The space \mathcal{HC} of the discrete scalar functions $\underset{\sim}{\phi}$ defined at the cell centers:

$$\mathcal{HC} = \left\{ \underset{\sim}{\phi} = (\phi_{i+\frac{1}{2}, j+\frac{1}{2}, k+\frac{1}{2}}) \right\}$$

and which is equipped with the natural inner product:

$$(\underset{\sim}{\phi}, \underset{\sim}{\phi}')_{\mathcal{HC}} = \sum_{i=1}^{M} \sum_{j=1}^{N} \sum_{k=1}^{K} \phi_{i-\frac{1}{2}, j-\frac{1}{2}, k-\frac{1}{2}} \phi'_{i-\frac{1}{2}, j-\frac{1}{2}, k-\frac{1}{2}} r_{i-\frac{1}{2}} \Delta r \Delta \theta \Delta z \quad (8)$$

- The space \mathcal{HL} of the discrete vector fields $\underline{\mathbf{W}}$ whose components are defined at the mid edges of the cells. The discrete vorticity belongs to this space.

$$\mathcal{HL} = \left\{ \underline{\mathbf{W}} = (\eta_{i+\frac{1}{2}, j, k}, \omega_{i, j+\frac{1}{2}, k}, \zeta_{i, j, k+\frac{1}{2}}) \right\}$$

- The space \mathcal{HN} of the discrete scalar function $\underset{\sim}{\psi}$ which are defined at the vertices (i, j, k) of the cells:

$$\mathcal{HN} = \left\{ \underset{\sim}{\psi} = (\psi_{i, j, k}) \right\}$$

The vertices of the original grid may be considered as the centers of cells for a dual grid which is the original one, shifted by half a mesh in each

direction. In this dual grid, the cells are parallelepipedic except those which *contain* the axis $r = 0$. The latter are cylinders with axis $r = 0$, located between the horizontal planes $k - \frac{1}{2}$ and $k + \frac{1}{2}$ and with an horizontal cross section which is defined on figure (4).

2.2 The divergence operator on \mathcal{HS}

Along the lines of Hyman and Shashkov [5], the discrete divergence is a mapping $\overline{\mathbf{D}}_S$ from \mathcal{HS} onto HC. It is defined by means of a discrete quadrature by the trapezoidal rule of the Gauss theorem over a cell $(i + \frac{1}{2}, j + \frac{1}{2}, k + \frac{1}{2})$. The value $\mathbf{D}_{i+\frac{1}{2},j+\frac{1}{2},k+\frac{1}{2}}$ of $\overline{\mathbf{D}}_S(\underline{\mathbf{U}})$ at the center of a cell non adjacent to the axis $r = 0$, satisfies the classical relation:

$$\begin{aligned} r_{i+\frac{1}{2}} \mathbf{D}_{i+\frac{1}{2},j+\frac{1}{2},k+\frac{1}{2}} \Delta r \Delta \theta \Delta z &= (r_{i+1} u_{i+1,j+\frac{1}{2},k+\frac{1}{2}} - r_i u_{i,j+\frac{1}{2},k+\frac{1}{2}}) \Delta \theta \Delta z \\ &+ (v_{i+\frac{1}{2},j+1,k+\frac{1}{2}} - v_{i+\frac{1}{2},j,k+\frac{1}{2}}) \Delta r \Delta z \\ &+ r_{i+\frac{1}{2}} (w_{i+\frac{1}{2},j+\frac{1}{2},k+1} - w_{i+\frac{1}{2},j+\frac{1}{2},k}) \Delta r \Delta \theta \end{aligned} \quad (9)$$

By the same approach, it is possible to define the discrete divergence at the center of a prismatic cell for which the axis $r = 0$ constitutes an edge:

$$\begin{aligned} r_{\frac{1}{2}} \mathbf{D}_{\frac{1}{2},j+\frac{1}{2},k+\frac{1}{2}} \Delta r \Delta \theta \Delta z &= (r_1 u_{1,j+\frac{1}{2},k+\frac{1}{2}}) \Delta \theta \Delta z \\ &+ (v_{\frac{1}{2},j+1,k+\frac{1}{2}} - v_{\frac{1}{2},j,k+\frac{1}{2}}) \Delta r \Delta z + r_{\frac{1}{2}} (w_{\frac{1}{2},j+\frac{1}{2},k+1} - w_{\frac{1}{2},j+\frac{1}{2},k}) \Delta r \Delta \theta \end{aligned} \quad (10)$$

which is nothing more than relation ((9)) written for $i = 0$ with the previous conventions $r_0 = 0$.

2.3 The gradient operator

Because the grid is orthogonal, the gradient operator $\overline{\mathbf{G}}$ is a mapping from HC onto \mathcal{HS} . It is defined as the negative adjoint of the discrete divergence operator with respect to the natural inner products in these spaces, i.e.

$$(\underset{\sim}{\phi}, \overline{\mathbf{D}}_S(\underline{\mathbf{U}}))_{\text{HC}} = -(\overline{\mathbf{G}}(\underset{\sim}{\phi}), \underline{\mathbf{U}})_{\mathcal{HS}}$$

After some algebra, this leads to the usual formulae for the radial, azimuthal and axial components of the discrete gradient of a scalar function ϕ which are reminded in appendix A.

2.4 The curl operator

The curl operator is a mapping $\overline{\mathbf{C}}_S$ from \mathcal{HS} onto \mathcal{HL} . It is defined by means of a discrete quadrature by the trapezoidal rule of the Stokes theorem along a suitable loop and the discrete vorticity components are defined at the edge centers and may be found in appendix A. It is straightforward to check that these equations are the classical second order centered finite differences approximations of the continuous components of the vorticity in cylindrical coordinates and are valid at any radial, azimuthal or axial mid-edge, except for the axial component of the vorticity on the axis $r = 0$ for which some care has to be taken. This is in our opinion, one of the key points to correctly deal with the axis in cylindrical coordinates.

2.5 Axial component of the vorticity on the axis

As usual, the axial component $Z_{k+\frac{1}{2}}$ of the vorticity on the axis $r = 0$ is computed by using a discrete version of the Stokes theorem along a suitable path which in this case, is the loop shown on figure (4):

$$Nr_{\frac{1}{2}} \Delta\theta \frac{\Delta r}{4} Z_{k+\frac{1}{2}} = r_{\frac{1}{2}} \Delta\theta \sum_{j=0}^{j=N-1} v_{\frac{1}{2},j,k+\frac{1}{2}}$$

Using $r_{\frac{1}{2}} = \Delta r/2$, this relation may be rewritten as:

$$Z_{k+\frac{1}{2}} = \frac{4}{\Delta r} \frac{1}{N} \sum_{j=0}^{j=N-1} v_{\frac{1}{2},j,k+\frac{1}{2}} = \frac{4}{\Delta r} \overline{v}_{\frac{1}{2},k+\frac{1}{2}} \quad (11)$$

where $\overline{v}_{\frac{1}{2},k+\frac{1}{2}}$ is the mean value of v along \mathcal{L} .

Remark:

It is straightforward to check that for these discrete operators, the standard vector analysis relation $\text{curl}(\text{grad})=0$ still holds:

$$\overline{\mathbf{C}}_S(\overline{\mathbf{G}}(\phi)) = 0 \quad \forall \phi \text{ in HC}$$

2.6 The divergence operator on \mathcal{HL}

It is also possible to define by means of Gauss theorem a divergence operator $\overline{\mathbf{D}}_L$ from \mathcal{HL} onto HN . For the cells of the dual grid which do not contain the

axis $r = 0$, the Gauss theorem for a vector $\underline{\mathbf{W}}$ in $\mathcal{H}\mathcal{L}$ reads:

$$\begin{aligned} r_i \bar{D}_{i,j,k} \Delta r \Delta \theta \Delta z &= (r_{i+\frac{1}{2}} \eta_{i+\frac{1}{2},j,k} - r_{i-\frac{1}{2}} \eta_{i-\frac{1}{2},j,k}) \Delta \theta \Delta z \\ &\quad + (\omega_{i,j+\frac{1}{2},k} - \omega_{i,j-\frac{1}{2},k}) \Delta r \Delta z + r_i (\zeta_{i,j,k+\frac{1}{2}} - \zeta_{i,j,k-\frac{1}{2}}) \Delta r \Delta \theta \end{aligned}$$

yielding the divergence:

$$\begin{aligned} \bar{D}_{i,j,k} &= \frac{1}{r_i} \left[\frac{r_{i+\frac{1}{2}} \eta_{i+\frac{1}{2},j,k} - r_{i-\frac{1}{2}} \eta_{i-\frac{1}{2},j,k}}{\Delta r} + \frac{\omega_{i,j+\frac{1}{2},k} - \omega_{i,j-\frac{1}{2},k}}{\Delta \theta} \right] \\ &\quad + \frac{\zeta_{i,j,k+\frac{1}{2}} - \zeta_{i,j,k-\frac{1}{2}}}{\Delta z} \end{aligned} \quad (12)$$

The volume of a cell containing the axis is $\mathcal{V} = N r_{1/2} \Delta \theta \frac{\Delta r}{4} \Delta z$. In this cell, the divergence satisfies:

$$\mathcal{V} \bar{D}_{0,k+\frac{1}{2}} = \mathcal{V} \frac{\zeta_{0,k+\frac{1}{2}} - \zeta_{0,k-\frac{1}{2}}}{\Delta z} + r_{1/2} \Delta \theta \Delta z \sum_{j=0}^{j=N-1} \eta_{\frac{1}{2},j,k}^1$$

yielding

$$\begin{aligned} \bar{D}_{0,k+\frac{1}{2}} &= \frac{\zeta_{0,k+\frac{1}{2}} - \zeta_{0,k-\frac{1}{2}}}{\Delta z} \\ &\quad + \frac{4}{\Delta r} \frac{1}{N} \sum_{j=0}^{j=N-1} \eta_{\frac{1}{2},j,k}^1 = \frac{\zeta_{0,k+\frac{1}{2}} - \zeta_{0,k-\frac{1}{2}}}{\Delta z} + \frac{4}{\Delta r} \bar{\eta}_{\frac{1}{2},k}^1 \end{aligned} \quad (13)$$

Remark 1 *It is easy to check that the usual vector relation $\text{div}(\text{curl})=0$ holds in the discrete case at every node of the dual grid:*

$$\bar{D}_L(\bar{\mathbf{C}}_S(\underline{\mathbf{U}})) = 0 \quad \forall \underline{\mathbf{U}} \text{ in } \mathcal{H}\mathcal{S}$$

2.7 The curl operator on $\mathcal{H}\mathcal{L}$

As in section §(2.4) it is possible by applying the Stokes theorem, to define a discrete curl operator $\bar{\mathbf{C}}_L$ which maps $\mathcal{H}\mathcal{L}$ onto $\mathcal{H}\mathcal{S}$. The formulae for the radial U , azimuthal V , and axial W components of $\bar{\mathbf{C}}_L(\underline{\mathbf{W}})$ are similar to relations (A.2), (A.3) and (A.4) for all the cell faces and read:

$$\begin{aligned} U_{i,j+\frac{1}{2},k+\frac{1}{2}} &= \frac{1}{r_i} \frac{\zeta_{i,j+1,k+\frac{1}{2}} - \zeta_{i,j,k+\frac{1}{2}}}{\Delta \theta} - \frac{\omega_{i,j+\frac{1}{2},k+1} - \omega_{i,j+\frac{1}{2},k}}{\Delta z} \\ V_{i+\frac{1}{2},j,k+\frac{1}{2}} &= \frac{\eta_{i+\frac{1}{2},j,k+1} - \eta_{i+\frac{1}{2},j,k}}{\Delta z} - \frac{\zeta_{i+1,j,k+\frac{1}{2}} - \zeta_{i,j,k+\frac{1}{2}}}{\Delta r} \\ W_{i+\frac{1}{2},j+\frac{1}{2},k} &= \frac{1}{r_{i+\frac{1}{2}}} \left[\frac{r_{i+1} \omega_{i+1,j+\frac{1}{2},k} - r_i \omega_{i,j+\frac{1}{2},k}}{\Delta r} - \frac{\eta_{i+\frac{1}{2},j+1,k} - \eta_{i+\frac{1}{2},j,k}}{\Delta \theta} \right] \end{aligned} \quad (14)$$

No specific relation is needed for particular cells unlike in §(2.4).

3 Discretization of differential second order operators

The use of a staggered grid allows us to define second order discrete operators as combinations of the previously defined discrete first order operators.

3.1 The diffusion operator

In order to use only first order operators, the diffusion term in the momentum equation is expressed as :

$$\tilde{\nabla}^2 \tilde{\mathbf{v}} = \nabla(\nabla \cdot \tilde{\mathbf{v}}) - \nabla \times \nabla \times \tilde{\mathbf{v}}$$

which allows us to use the discrete divergence, grad and curl operators defined in the previous sections. From this discrete point of view, the associated discrete diffusion term belong to \mathcal{HS} , i.e. its discrete components are defined in the same locations as the velocity components. We now distinguish between the regular cells and the axis cells.

3.1.1 Regular Cells

For the sake of simplicity, we will consider the continuous case for cells not adjacent to the axis, since we have noticed that in this case, the discrete operators were exactly similar to the continuous operators. The components of the curl of a vector in cylindrical coordinates are:

$$\eta = \frac{1}{r} \frac{\partial w}{\partial \theta} - \frac{\partial v}{\partial z} ; \omega = \frac{\partial u}{\partial z} - \frac{\partial w}{\partial r} ; \zeta = \frac{1}{r} \left(\frac{\partial(rv)}{\partial r} - \frac{\partial u}{\partial \theta} \right)$$

Taking the curl of the curl and inserting the continuity equation

$$\frac{\partial(rv)}{\partial r} + \frac{\partial v}{\partial \theta} + r \frac{\partial w}{\partial z} = 0$$

yields:

$$(\nabla_{\sim}^2 \mathbf{v})_r = \frac{\partial}{\partial r} \left(\frac{1}{r} \frac{\partial(ru)}{\partial r} \right) + \frac{1}{r^2} \frac{\partial^2 u}{\partial \theta^2} + \frac{\partial^2 u}{\partial z^2} + \frac{\partial}{\partial \theta} \left[\frac{1}{r^2} \frac{\partial(rv)}{\partial r} - \frac{\partial}{\partial r} \left(\frac{v}{r} \right) \right] \quad (15)$$

$$(\nabla_{\sim}^2 \mathbf{v})_\theta = \frac{\partial}{\partial r} \left(\frac{1}{r} \frac{\partial(rv)}{\partial r} \right) + \frac{1}{r^2} \frac{\partial^2 v}{\partial \theta^2} + \frac{\partial^2 v}{\partial z^2} - \frac{\partial}{\partial \theta} \left[\frac{1}{r^2} \frac{\partial(ru)}{\partial r} - \frac{\partial}{\partial r} \left(\frac{u}{r} \right) \right] \quad (16)$$

$$(\nabla_{\sim}^2 \mathbf{v})_z = \frac{1}{r} \frac{\partial}{\partial r} \left(r \frac{\partial w}{\partial r} \right) + \frac{1}{r^2} \frac{\partial^2 w}{\partial \theta^2} + \frac{\partial^2 w}{\partial z^2} \quad (17)$$

The terms in brackets in equations (15) and (16) gives after simplification the terms usually found in textbooks, namely:

$$\frac{2}{r^2} \frac{\partial v}{\partial \theta} \quad \text{and} \quad - \frac{2}{r^2} \frac{\partial u}{\partial \theta}$$

However, it is easy to check that thanks to the staggered arrangement, the apparently more complicated form in brackets is more suitable for a discretization on a staggered grid and therefore, will be retained in the discretization.

3.1.2 Axis cells

We revert now to the discrete mimetic difference operators. The procedure is the same as before. The discrete relations for the vorticity components on the edges of a prismatic cell are inserted in relations (14). The resulting relation is then transformed by inserting the discrete continuity equation (10) yielding two relations, one for the radial component CCU and the other for the azimuthal CCV. In the former, the only specific term is the following:

$$\begin{aligned} \text{CCU}_{1,j+\frac{1}{2},k+\frac{1}{2}} &= \frac{1}{\Delta r} \left(\frac{1}{r_{\frac{3}{2}}} \frac{r_2 u_{2,j+\frac{1}{2},k+\frac{1}{2}} - r_1 u_{1,j+\frac{1}{2},k+\frac{1}{2}}}{\Delta r} \right) \\ &\quad - \frac{1}{r_1^2} \delta_{\theta\theta}(u)_{1,j+\frac{1}{2},k+\frac{1}{2}} - \delta_{zz}(u)_{1,j+\frac{1}{2},k+\frac{1}{2}} \\ &\quad - \frac{1}{\Delta r} \left[\left(\frac{r_{\frac{3}{2}}}{r_1^2} - \frac{1}{r_{\frac{3}{2}}} \right) \frac{v_{\frac{3}{2},j+1,k+\frac{1}{2}} - v_{\frac{3}{2},j,k+\frac{1}{2}}}{\Delta \theta} \right. \\ &\quad \left. - \left(\frac{r_{\frac{1}{2}}}{r_1^2} - \frac{1}{r_{\frac{1}{2}}} \right) \frac{v_{\frac{1}{2},j+1,k+\frac{1}{2}} - v_{\frac{1}{2},j,k+\frac{1}{2}}}{\Delta \theta} \right] \end{aligned} \quad (18)$$

$$\begin{aligned} \text{CCV}_{\frac{1}{2},j,k+\frac{1}{2}} &= \frac{1}{\Delta r} \left(\frac{1}{r_1} \frac{r_{\frac{3}{2}} v_{\frac{3}{2},j,k+\frac{1}{2}} - r_{\frac{1}{2}} v_{\frac{1}{2},j,k+\frac{1}{2}}}{\Delta r} - Z_{k+\frac{1}{2}} \right) \\ &\quad - \frac{1}{r_{\frac{1}{2}}^2} \delta_{\theta\theta}(v)_{\frac{1}{2},j,k+\frac{1}{2}} - \delta_{zz}(v)_{\frac{1}{2},j,k+\frac{1}{2}} \\ &\quad + \frac{1}{\Delta r} \left[\left(\frac{r_1}{r_{\frac{1}{2}}^2} - \frac{1}{r_1} \right) \frac{u_{1,j+\frac{1}{2},k+\frac{1}{2}} - u_{1,j-\frac{1}{2},k+\frac{1}{2}}}{\Delta \theta} \right] \end{aligned} \quad (19)$$

In these relations, $\delta_{\theta\theta}$ and δ_{zz} stands for the standard second order centered approximation of the second derivatives with respect to θ and z . Noteworthy is the fact that thanks to a rigorous application of the Gauss and Stokes theorems, no artificial boundary conditions are needed on the axis $r = 0$ where actually, they would be meaningless.

3.2 The scalar Laplace operator

We apply the same technique to the $\text{div}(\text{grad})$ operator which appears in the projection step of the time marching procedure in §(1). For the sake of simplicity, only the discretized version of

$$\frac{1}{r} \frac{\partial}{\partial r} \left(r \frac{\partial \phi}{\partial r} \right)$$

will be given here:

– at the center of a regular cell

$$\frac{1}{r_{i+\frac{1}{2}}} \frac{1}{\Delta r} \left(r_{i+1} \frac{\phi_{i+\frac{3}{2},j+\frac{1}{2},k+\frac{1}{2}} - \phi_{i+\frac{1}{2},j+\frac{1}{2},k+\frac{1}{2}}}{\Delta r} - r_i \frac{\phi_{i+\frac{1}{2},j+\frac{1}{2},k+\frac{1}{2}} - \phi_{i-\frac{1}{2},j+\frac{1}{2},k+\frac{1}{2}}}{\Delta r} \right)$$

– at the center of an axis cell

$$\frac{1}{r_{\frac{1}{2}}} \frac{1}{\Delta r} \left(r_1 \frac{\phi_{\frac{3}{2},j+\frac{1}{2},k+\frac{1}{2}} - \phi_{\frac{1}{2},j+\frac{1}{2},k+\frac{1}{2}}}{\Delta r} \right)$$

3.3 Well posedness of the discrete systems

One of the main advantages of using mimetic finite difference operators derives from the two following remarks:

- By construction, the discrete divergence and gradient operators are negative adjoint with respect to the different inner products defined in section (2). Thus, the discrete system (3)–(4) may be written in the following form:

$$\underline{\underline{\mathbf{A}}} \underline{\underline{\mathbf{U}}} + \underline{\underline{\mathbf{B}}}^t \underline{\underline{\mathbf{P}}} = \underline{\underline{\mathbf{F}}} \quad (20)$$

$$\underline{\underline{\mathbf{B}}} \underline{\underline{\mathbf{U}}} = 0 \quad (21)$$

where $\underline{\underline{\mathbf{U}}}$ stands for the discrete velocity, $\underline{\underline{\mathbf{P}}}$ stands for the discrete pressure, $\underline{\underline{\mathbf{F}}}$ stands for the discrete source terms, $\underline{\underline{\mathbf{B}}}$ stands for the discrete divergence operator and $\underline{\underline{\mathbf{A}}}$ stands for the discrete Helmholtz operator. It is of the

utmost importance to note that, thanks to the adjointness property, the operator $\underline{\mathbf{A}}$ is self-adjoint and positive definite.

- If we assume that the computational domain Ω is simply connected (this is the case for the flow under consideration), it is a simple matter of algebra to check that the kernel of the discrete gradient operator $\underline{\mathbf{B}}^t$ reduces to the constant mode.

These remarks classically ensure that the discrete system is well posed and in particular that the computed pressure field is free of spurious checkerboard oscillations. This is, within a finite differences context, analogous to the LBB condition that is well known in the finite element community [18].

4 The Non Linear Terms

Since the non linear terms do not contribute to energy production in the continuum incompressible Navier–Stokes equations, we have chosen to use a discrete scheme which has the same property in the discrete sense, at least when the non linear terms are implicitly treated. Following [17], we decided to use the rotational form $\underline{\boldsymbol{\omega}} \times \underline{\boldsymbol{v}}$ of the convective terms that seems to be adapted to this objective. Within the discrete framework of §(2), the discrete counterparts $\underline{\mathbf{U}}$ of the velocity and $\underline{\mathbf{N}}$ of the non linear terms belong to \mathcal{HS} and must satisfy the orthogonality relation:

$$(\underline{\mathbf{U}}, \underline{\mathbf{N}})_{\mathcal{HS}} = 0 \quad (22)$$

A convenient discretization for the radial component N^1 of $\underline{\mathbf{N}}$ is then:

$$N_{i,j+\frac{1}{2},k+\frac{1}{2}}^1 = \frac{1}{2} \left[\omega_{i,j+\frac{1}{2},k+1} \bar{w}_{i,j+\frac{1}{2},k+1} + \omega_{i,j+\frac{1}{2},k} \bar{w}_{i,j+\frac{1}{2},k} - \zeta_{i,j+1,k+\frac{1}{2}} \bar{v}_{i,j+1,k+\frac{1}{2}} - \zeta_{i,j,k+\frac{1}{2}} \bar{v}_{i,j,k+\frac{1}{2}} \right] \quad (23)$$

In this relation, \bar{w} stands for the radius weighted average:

$$\bar{w}_{i,j+\frac{1}{2},k} = \frac{r_{i+\frac{1}{2}} w_{i,j+\frac{1}{2},k} + r_{i-\frac{1}{2}} w_{i,j-\frac{1}{2},k}}{2r_i}$$

In appendix B, similar relations for the azimuthal and axial components are given and after some algebra, it is possible to check that the orthogonality relation (22) is actually satisfied.

5 Some Implementation Considerations

5.1 Treatment of the periodicity in the azimuthal direction

In our computations, any function f is expanded in truncated Fourier series over N modes:

$$f(r, \theta, z) = \frac{\hat{f}_0}{\sqrt{2}} + \sum_{m=1}^{m=N/2-1} \hat{f}_m(r, z) \cos(m\theta) + \hat{f}_{N-m}(r, z) \sin(m\theta)$$

and the finite differences in the θ direction are replaced by:

$$\begin{aligned} \frac{\partial}{\partial \theta} : \hat{f}_m &\longrightarrow -m \hat{f}_{N-m} \\ \frac{\partial}{\partial \theta} : \hat{f}_{N-m} &\longrightarrow m \hat{f}_m \\ \frac{\partial^2}{\partial \theta^2} : \hat{f}_m &\longrightarrow -m^2 \hat{f}_m \end{aligned}$$

The non-linear terms are classically evaluated in a pseudospectral way [19] with a dealiasing procedure over $3N/2$ modes.

5.2 The axial vorticity on the axis $r = 0$

The axial vorticity $Z_{k+\frac{1}{2}}$ on the axis is part of the v -equation in the axis cells (see relation (19)) and was shown in §(2.5) to be related to the azimuthal velocity by:

$$Z_{k+\frac{1}{2}} = \frac{4}{\Delta r} \bar{v}_{1/2, k+\frac{1}{2}}$$

where $\bar{v}_{\frac{1}{2}, k+\frac{1}{2}}$ is the mean value with respect to j of the $v_{\frac{1}{2}, j, k+\frac{1}{2}}$. Because $Z_{k+\frac{1}{2}}$ does not depend on any azimuthal station, only its $m = 0$ mode \hat{Z}_0 is non zero. Moreover, thanks to the usual properties of the Fourier coefficients \hat{Z}_m , the following relations hold:

$$\begin{aligned} \hat{Z}_0|_{k+\frac{1}{2}} &= \frac{4}{\Delta r} \hat{v}_0|_{\frac{1}{2}, k+\frac{1}{2}} \\ \hat{Z}_m|_{k+\frac{1}{2}} &= 0 \quad \forall m > 0 \end{aligned}$$

5.3 Boundary conditions

5.3.1 Momentum equation

The boundary conditions are of homogeneous Dirichlet type for the fluctuating velocity components. For the sake of brevity, we only consider the case of the discrete axial second order derivative $\delta^2/\delta z^2$ of the unknowns in the vicinity of the lower rotating lid $z = 0$ whose Fourier coefficients are written as:

$$\begin{aligned}\left.\frac{\delta^2 \hat{u}}{\delta z^2}\right|_{i, \frac{1}{2}} &= \frac{1}{\Delta z} \left(\frac{\hat{u}_{i, \frac{3}{2}} - \hat{u}_{i, \frac{1}{2}}}{\Delta z} - \frac{2}{\Delta z} \hat{u}_{i, \frac{1}{2}} \right) \\ \left.\frac{\delta^2 \hat{v}}{\delta z^2}\right|_{i, \frac{1}{2}} &= \frac{1}{\Delta z} \left(\frac{\hat{v}_{i, \frac{3}{2}} - \hat{v}_{i, \frac{1}{2}}}{\Delta z} - \frac{2}{\Delta z} \hat{v}_{i, \frac{1}{2}} \right) \\ \left.\frac{\delta^2 \hat{w}}{\delta z^2}\right|_{i, 1} &= \frac{1}{\Delta z} \left(\frac{\hat{w}_{i, 2} - \hat{w}_{i, 1}}{\Delta z} - \frac{\hat{w}_{i, 1}}{\Delta z} \right)\end{aligned}$$

The boundary conditions at $r = 1$ are derived in a similar way

5.3.2 Poisson equation

In the projection step (see §(1)), the boundary conditions (6) for the auxiliary function ϕ are homogeneous Neumann conditions. Since the scalar unknowns are located at the cell centers, the boundary conditions are treated in a natural way, e.g.

$$\left.\frac{\delta^2 \hat{\phi}}{\delta z^2}\right|_{i, \frac{1}{2}} = \frac{1}{\Delta z} \left(\frac{\hat{\phi}_{i, \frac{3}{2}} - \hat{\phi}_{i, \frac{1}{2}}}{\Delta z} \right)$$

5.4 Resolution of the discrete systems

Because of the geometry and of the used grid, the N discrete independent systems, one for each mode, arising from the Fourier expansion are in tensor form and are therefore solved by means of a partial diagonalization in the axial direction [20]. For the scalar Poisson equation and the $m = 0$ modes of the momentum equation, this technique leads to the resolution of a set of independent tridiagonal systems. In the case of $m \neq 0$ modes of the momentum equation, it leads to the resolution of pentadiagonal systems for \hat{u}_m and \hat{v}_{N-m} on one hand and for \hat{u}_{N-m} and \hat{v}_m on the other hand. These systems arise from the coupling between the radial and the azimuthal components of the velocity in the diffusion operator (see relations (15) and (16)). Finally, thanks to the uniformity of the grid, this diagonalization and the associated change

of basis, are performed by means of a Fast Fourier Transform, dramatically increasing the efficiency of the numerical code.

6 Validation

In this section we present results concerning the two main kind of confined flows that may be found in configurations possessing the $SO(2)$ symmetry: with and without a non zero flow through the origin. Both possibilities are examined in the sequel.

7 Flow in a circular lid driven cavity

In order to stress the axis treatment, the ability of the proposed technique to deal with flows having a non vanishing velocity through the origin is investigated. For this purpose, the two dimensional flow inside a circular disk of radius R_0 generated by a rotation of the boundary has been considered. More specifically, the boundary conditions along the circle $r = R_0$ are:

$$u = 0 ; v = -\sin(\theta - \theta_0)$$

where θ_0 is an arbitrary angle. These boundary conditions generate a structure similar to a dipolar vortex with an almost uniform axial flow along the $\theta = \theta_0$ direction through the origin.

The computations reported here were performed for $Re = 400$ and different values of θ_0 . Streamlines for two such flows are displayed in figure 5, clearly showing a non zero flow through the origin. Moreover, the axial vorticity at the origin was found to be zero (within machine errors), indicating an almost uniform flow in the vicinity of the origin.

8 Flow in a cylindrical tank with a rotating lid

As an example of flows with zero flow through the origin, the case of the flow in a cylindrical tank with a rotating lid has been investigated. This kind of flow has been extensively considered in the literature and numerous numerical and experimental results are available, e.g. [1,9–11,8]. The methodology that underlies all the computations presented in this paper consists in two main steps and is essentially the same as in Daube and Le Quéré [21]:

- For each selected value of Re and of the aspect ratio A , an axisymmetric steady base state is computed along the lines of a methodology proposed by Tuckerman [22].
- The equations are then cast in perturbation form with respect to this base flow and integrated, in linearized or in non linear form, starting from initial conditions that may be either a random field or an instantaneous field from a previous computation. In the sequel, E' will denote the kinetic energy of the perturbation and E_0 the kinetic energy of the base flow.

This section is first devoted to the computation of the 3D linearized evolution around a steady axisymmetric base state. Our results are compared with those of Gelfgat [15] and turn out to be in excellent agreement with these results. In a second part, attention is focused on the axisymmetry breaking and on the onset of a rotating wave and our results are compared to those of Marques and Lopez [13].

8.1 *Linearized computations*

The numerical method was first validated by computing axisymmetric steady solutions which were compared to those found in the literature. The results are not reported here but the agreement was found excellent. In order to validate the 3D characteristics of the code, some linearized computations were then carried out in order to check if the linear thresholds obtained by [15] could be recovered. Here, we give only some results in the case $A = 1$ which were obtained on an uniform $101 \times 32 \times 101$ grid in (r, θ, z) . The time evolution of the kinetic energy E' (normalized by the kinetic energy E_0 of the base flow) of the $m = 2$ Fourier mode is displayed on figure (6), for Reynolds numbers varying from 2430 to 2460 by increments of 10. It shows that this mode becomes linearly unstable for $Re \simeq 2450$. The time evolution of E'/E_0 for the Fourier modes $m = 0, \dots, 5$ is displayed on figure (7) for $Re = 2550$. It is clearly seen that the $m = 2$ mode is the only one unstable. These results are in excellent agreement with Gelfgat's results [15].

8.2 *Influence of the grid*

The dependence of the critical Reynolds number on the grid size $\Delta r = 1/M$ was then analyzed. For this purpose, three different grids, all with the same number of nodes $N=32$ in the azimuthal direction, were used. For each grid, the critical Reynolds number Re_c is computed by the following procedure:

- (1) For a given Reynolds number Re , the growth rate σ of the perturbation is estimated from the time evolutions such as the one depicted in figure

- (6),
- (2) Since the growth rate σ is known to be proportional to $(\text{Re} - \text{Re}_c)^{-1}$, an estimation of Re_c is computed by linear extrapolation to zero of the $1/\sigma$ values.

The computed values of the critical Reynolds number are reported on fig (8). The dependence on Δr^2 of this critical value can be observed, a fact which allows us to extrapolate for $\Delta r = 0$, yielding a value of 2473 which is very close to the value 2471 obtained by Gelfgat [15] with a spectral technique. Noteworthy is the fact that with $N_r = N_z = 100$ grid points in each direction, the computed critical value is 2447 differing by less than 1% from the exact value.

9 Axisymmetry breaking and onset of a rotating wave

The main point is that if the bifurcation breaks the axisymmetry, it gives rise to a rotating wave as explained for instance by Knobloch [23] and numerically evidenced by Marquès and Lopez [13]. It was therefore essential that this feature could be recovered. All the computations which are reported in this section were carried out in perturbation form, starting from a randomly distributed initial perturbation on a $101 \times 32 \times 301$ uniform grid in (r, θ, z) and are for the case $A = 3$ and $\text{Re} = 2850$.

9.1 Axisymmetry breaking

On figure (9), the time evolutions of the kinetic energy ratio E'/E_0 for the first ten Fourier modes are displayed. It shows that after a long transient stage, the energies of the $m = 4$ mode, and (by non linear interactions) of the $m = 0$ and $m = 8$ modes saturate at a finite constant level of energy (a fact which is consistent with the occurrence of a rotating wave) whereas all the other modes are damped. Note also that these levels are low, indicating that the three dimensional effects are weak. Because of the large amount of CPU time involved in these computations, we did not try to perform any further accurate determination of the critical Reynolds number and therefore, we can only say is that our results are consistent with [13]. For the same purpose of comparison, are also shown:

- on figure (10): isovalue lines of the axial component w' of the fluctuating velocity and of the axial component w of the total velocity in the plane $z = 0.8A$. The alternating dark (≥ 0) and clear (≤ 0) patches of the fluctuating velocity and the square structure for the total component clearly

show the occurrence of the $m = 4$ Fourier mode.

- on figures (11)(a) to (11)(d): isovalue lines of the total axial component w in different meridional planes. As noticed in [13], these pictures show that the three dimensional effects are weak and mainly located in the vicinity of the sidewall.

9.2 Transition to unsteadiness and onset of a rotating wave

As the Reynolds number is increased, the flow undergoes a transition from a steady axisymmetric state to a full 3D unsteady one. On figure 12, the time evolution of the total axial component w at two locations differing only by an azimuthal angle of $\pi/8$ is displayed, showing that the flow is periodic of period $T \simeq 2.35$ revolutions unit times and also that, due to the $m = 4$ dominant Fourier mode, the two signals are out of phase.

This unsteadiness occurs through the onset of a rotating wave. A first hint of this phenomena was noticed in the previous section since the kinetic energy of each saturated Fourier mode was shown to be asymptotically constant. It is confirmed by figures 13 displaying a temporal sequence of w -isolines in the plane $z = 0.8H$ at times indicated on figure 12 by the + symbols. The rotating wave is clearly seen by the fact that the square shaped pattern of each figure is derived from the previous by a rotation of constant angle. Since the dominant azimuthal Fourier mode is $m = 4$, the period T_w of the rotating wave is equal to $4 \times T$ in revolution time units. Reminding that the counter clockwise rotating disk is located at $z = 0$ and that these pictures are seen from above, we therefore infer that the wave is rotating in the same direction as the disk but at a lower angular velocity.

Conclusions

In this paper we have derived a rigorous finite differences framework for cylindrical coordinates on uniform rectangular grids. We would like to stress once more the fact that because we only use discrete versions of the Stokes and of the divergence theorems, no particular assumption on the regularity of the Fourier coefficients was necessary in the vicinity of the axis $r = 0$. Another important point is that the discrete divergence and gradient operators are negative adjoint with respect to the usual inner product therefore ensuring that the discrete systems are well posed, i.e. the pressure field is free of spurious checkerboard oscillations. In addition, the nonlinear terms have been discretized in such a way that they are energetically neutral, a fact which would ensure the unconditional \mathbb{L}^2 stability provided that a temporal scheme

with an implicit treatment of $\tilde{\boldsymbol{v}}$ in the $\tilde{\boldsymbol{\omega}} \times \tilde{\boldsymbol{v}}$ term is used.

The results presented for the first bifurcation of flows in enclosed cylinder with aspect ratio $A \geq 1$, are in excellent agreement with the available literature; it shows that the methodology can be used to study many other similar configurations such as rotor–stator flows, Taylor–Couette flows. However, in order to deal with larger values of the Reynolds number, non uniform, but still rectangular, grids in the (r, z) plane will have to be considered in the future works. Actually, extension of the present framework to non uniform rectangular grids does not raise any particular problems and is in progress.

Acknowledgments:

The computations were performed on the NEC-SX5 supercomputer at IDRIS, the super computing center of the french CNRS. CPU resources were provided under project number 1312.

A Discrete formulæ

A.1 The discrete gradient operator

$$\overline{\mathbf{G}}(\underset{\sim}{\phi}) = \frac{1}{r_{i+\frac{1}{2}}} \begin{cases} \frac{\phi_{i+\frac{1}{2},j+\frac{1}{2},k+\frac{1}{2}} - \phi_{i-\frac{1}{2},j+\frac{1}{2},k+\frac{1}{2}}}{\Delta r} & \text{at node } (i, j + \frac{1}{2}, k + \frac{1}{2}) \\ \frac{\phi_{i+\frac{1}{2},j+\frac{1}{2},k+\frac{1}{2}} - \phi_{i+\frac{1}{2},j-\frac{1}{2},k+\frac{1}{2}}}{\Delta \theta} & \text{at node } (i + \frac{1}{2}, j, k + \frac{1}{2}) \\ \frac{\phi_{i+\frac{1}{2},j+\frac{1}{2},k+\frac{1}{2}} - \phi_{i+\frac{1}{2},j+\frac{1}{2},k-\frac{1}{2}}}{\Delta z} & \text{at node } (i + \frac{1}{2}, j + \frac{1}{2}, k) \end{cases} \quad (\text{A.1})$$

A.2 The discrete curl operator

The radial component η of the discrete vorticity $\overline{\mathbf{C}}_S(\mathbf{U})$ is defined at the mid-edge $(i + \frac{1}{2}, j, k)$ by applying the Stokes theorem along the loop \mathcal{L} defined on figure (3)-a:

$$\eta_{i+\frac{1}{2},j,k} r_{i+\frac{1}{2}} \Delta \theta \Delta z = \Delta z (w_{i+\frac{1}{2},j+\frac{1}{2},k} - w_{i+\frac{1}{2},j-\frac{1}{2},k}) - r_{i+\frac{1}{2}} \Delta \theta (v_{i+\frac{1}{2},j+\frac{1}{2},k+\frac{1}{2}} - v_{i+\frac{1}{2},j+\frac{1}{2},k-\frac{1}{2}})$$

yielding

$$\eta_{i+\frac{1}{2},j,k} = \frac{1}{r_{i+\frac{1}{2}}} \frac{w_{i+\frac{1}{2},j+\frac{1}{2},k} - w_{i+\frac{1}{2},j-\frac{1}{2},k}}{\Delta \theta} - \frac{v_{i+\frac{1}{2},j+\frac{1}{2},k+\frac{1}{2}} - v_{i+\frac{1}{2},j+\frac{1}{2},k-\frac{1}{2}}}{\Delta z} \quad (\text{A.2})$$

By applying the Stokes theorem along the loop \mathcal{L} defined on figure (3)-b, the azimuthal component ω of the vorticity is defined at the mid-edge $(i, j + \frac{1}{2}, k)$ by:

$$\omega_{i,j+\frac{1}{2},k} = \frac{u_{i,j+\frac{1}{2},k+\frac{1}{2}} - u_{i,j+\frac{1}{2},k-\frac{1}{2}}}{\Delta z} - \frac{w_{i+\frac{1}{2},j+\frac{1}{2},k} - w_{i-\frac{1}{2},j+\frac{1}{2},k}}{\Delta r} \quad (\text{A.3})$$

and by applying the Stokes theorem along the loop \mathcal{L} defined on figure (3)-c, the axial component ζ of the vorticity at a midpoint $(i, j, k + \frac{1}{2})$ of a vertical edge not on the axis ($i \neq 0$), reads:

$$\zeta_{i,j,k+\frac{1}{2}} = \frac{1}{r_i} \left[\frac{r_{i+\frac{1}{2}} v_{i+\frac{1}{2},j,k+\frac{1}{2}} - r_{i-\frac{1}{2}} v_{i-\frac{1}{2},j,k+\frac{1}{2}}}{\Delta r} - \frac{u_{i,j+\frac{1}{2},k+\frac{1}{2}} - u_{i,j-\frac{1}{2},k+\frac{1}{2}}}{\Delta \theta} \right] \quad (\text{A.4})$$

B Discretization of the non linear terms

Along the lines of the notations in §(4), a convenient discretization for the axial component N^3 of the non linear terms $\underline{\mathbf{N}}$ is :

$$N_{i+\frac{1}{2},j+\frac{1}{2},k}^3 = \frac{1}{2} \left[\omega_{i,j+\frac{1}{2},k} \bar{u}_{i,j+\frac{1}{2},k} + \omega_{i+1,j+\frac{1}{2},k} \bar{u}_{i+1,j+\frac{1}{2},k} - \eta_{i+\frac{1}{2},j+1,k} \bar{v}_{i+\frac{1}{2},j+1,k} - \eta_{i+\frac{1}{2},j,k} \bar{v}_{i+\frac{1}{2},j,k} \right] \quad (\text{B.1})$$

where $\bar{u}_{i,j+\frac{1}{2},k}$ stands for the arithmetic mean of $u_{i,j+\frac{1}{2},k-\frac{1}{2}}$ and $u_{i,j+\frac{1}{2},k+\frac{1}{2}}$ and $\bar{v}_{i+\frac{1}{2},j,k}$ stands for the arithmetic mean of $v_{i+\frac{1}{2},j,k-\frac{1}{2}}$ and $v_{i+\frac{1}{2},j,k+\frac{1}{2}}$.

A convenient discretization for the azimuthal component N^2 of the non linear terms $\underline{\mathbf{N}}$ is :

$$N_{i+\frac{1}{2},j,k+\frac{1}{2}}^2 = \frac{1}{2} \left[\zeta_{i,j,k+\frac{1}{2}} \bar{u}_{i,j,k+\frac{1}{2}} + \zeta_{i+1,j+\frac{1}{2},k} \bar{u}_{i+1,j,k+\frac{1}{2}} - \eta_{i+\frac{1}{2},j,k+1} \bar{w}_{i+\frac{1}{2},j,k+1} - \eta_{i+\frac{1}{2},j,k} \bar{w}_{i+\frac{1}{2},j,k} \right] \quad (\text{B.2})$$

where $\bar{u}_{i,j,k+\frac{1}{2}}$ stands for the arithmetic mean of $u_{i,j-\frac{1}{2},k+\frac{1}{2}}$ and $u_{i,j+\frac{1}{2},k+\frac{1}{2}}$ and $\bar{w}_{i+\frac{1}{2},j,k}$ stands for the arithmetic mean of $w_{i+\frac{1}{2},j-\frac{1}{2},k}$ and $w_{i+\frac{1}{2},j+\frac{1}{2},k}$.

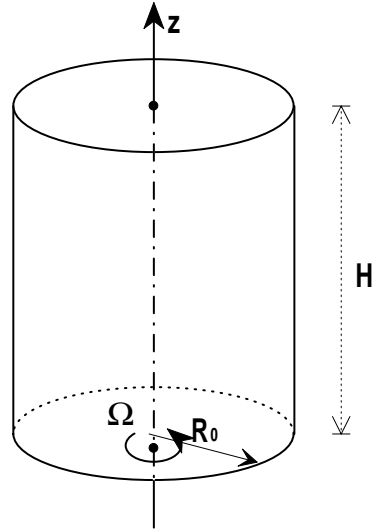


Fig. 1. sketch of the configuration

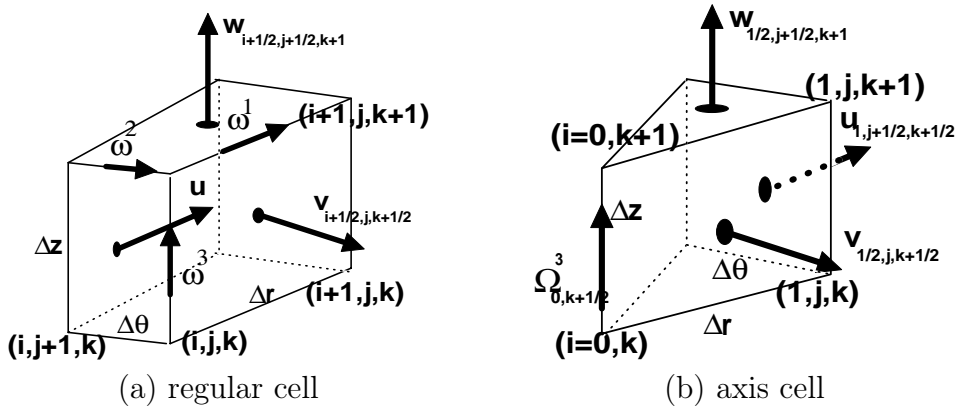


Fig. 2. The MAC grid

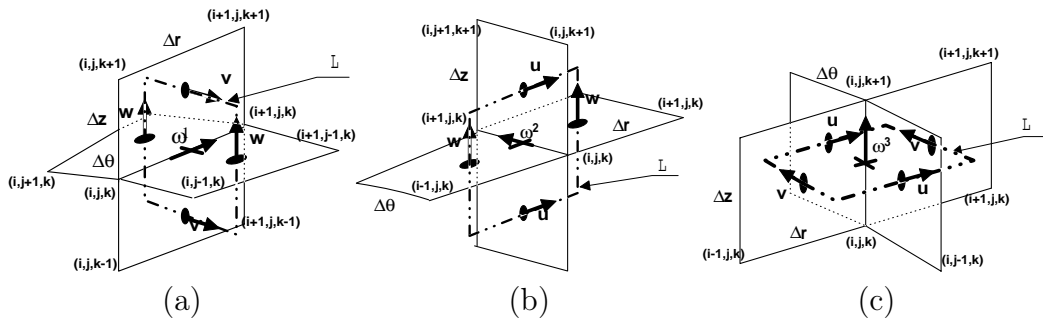


Fig. 3. Loops along which the Stokes theorem is applied in order to compute the (a) radial component, (b) azimuthal component, (c) axial component of the vorticity

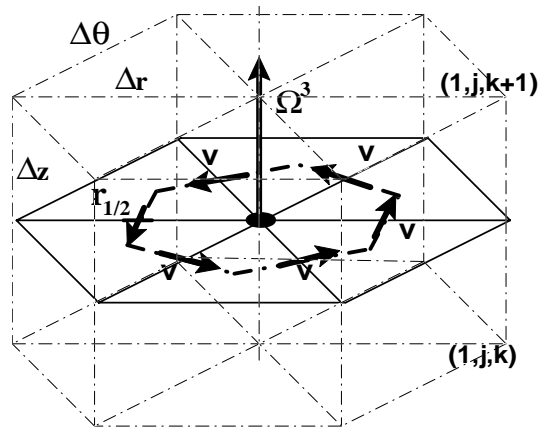


Fig. 4. Loop to compute the axial component $Z_{k+\frac{1}{2}}$ of the vorticity at a point on the axis $r = 0$ and in the plane $z = (k + \frac{1}{2})\Delta z$

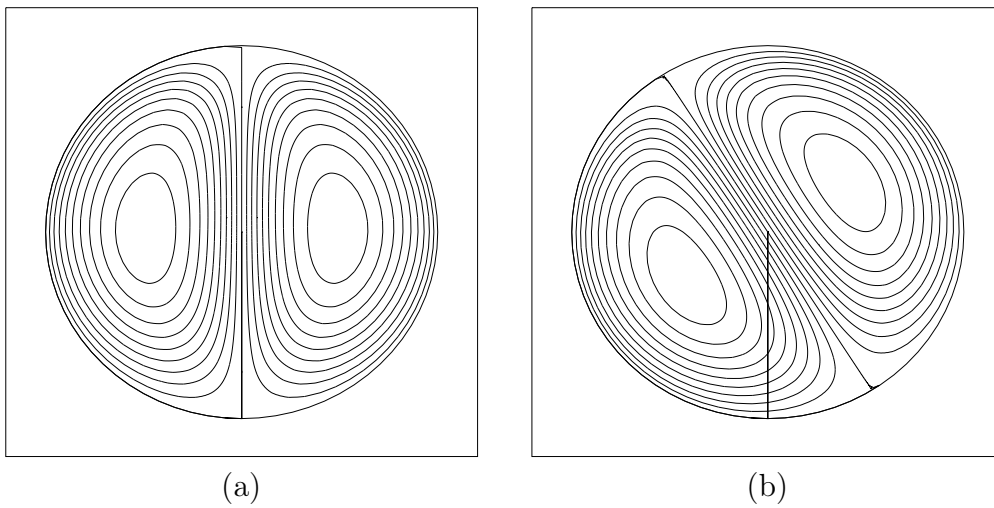


Fig. 5. streamlines for the circular lid driven cavity at $Re = 400$; (a) $\theta_0 = 0$ (b) $\theta_0 = 32$ degrees

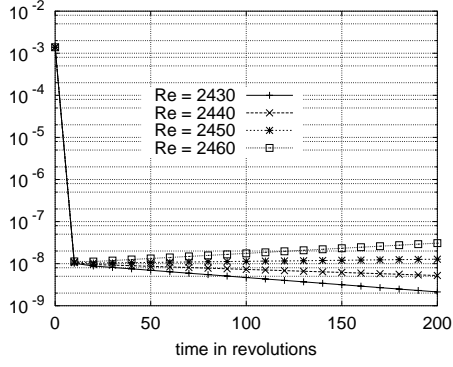


Fig. 6. time evolution of the normalized kinetic energy E'/E_0 of the $m = 2$ Fourier mode for $A = 1$ and different values of the Reynolds number

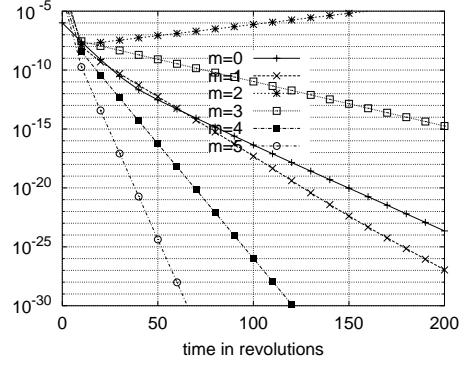


Fig. 7. time evolution of the normalized kinetic energy E'/E_0 of different Fourier modes for $A = 1$ and Reynolds number = 2550

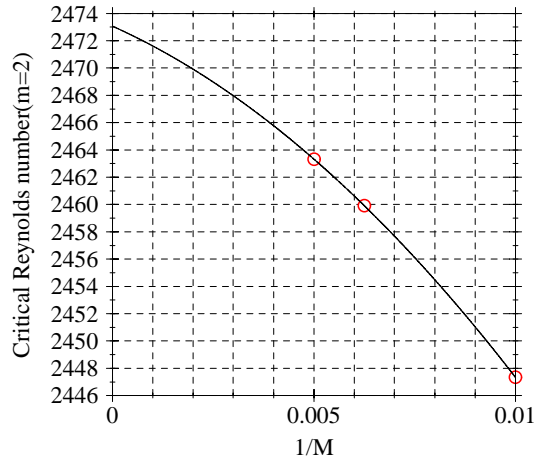


Fig. 8. critical linear threshold as computed for three different grids: $101 \times 32 \times 101$, $161 \times 32 \times 161$, $201 \times 32 \times 201$ in (r, θ, z) and extrapolated to zero

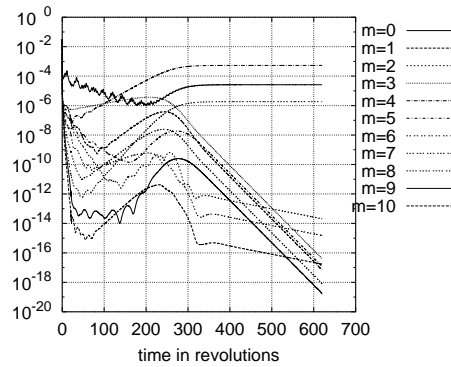


Fig. 9. Time evolution of the kinetic energy of Fourier modes $m = 0$ to $m = 10$ for $Re = 2850$; $A = 3$

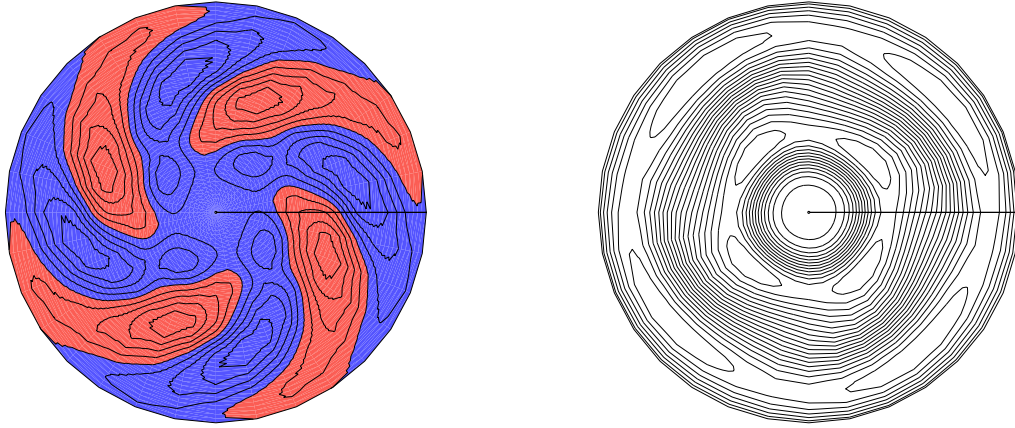


Fig. 10. isolines of the axial velocity in the plane $z = 0.8A$; left: fluctuating axial velocity ; right: total axial velocity

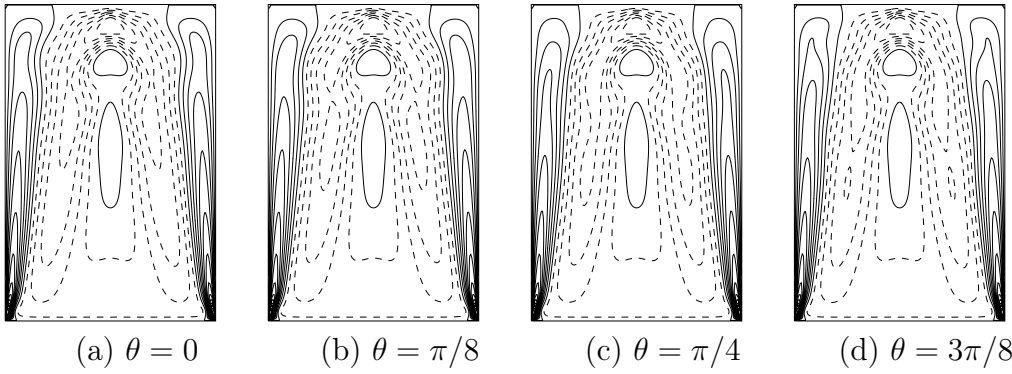


Fig. 11. iso-lines of w in meridional planes for azimuthal locations as indicated. The dashed lines are for negative values of w

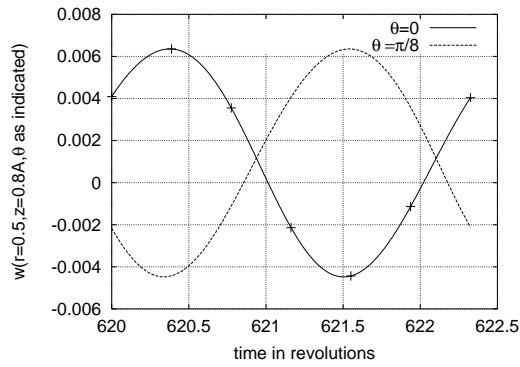


Fig. 12. Time evolution of the total axial component w of the velocity at two different points. The + symbols correspond to the different patterns of the next figure

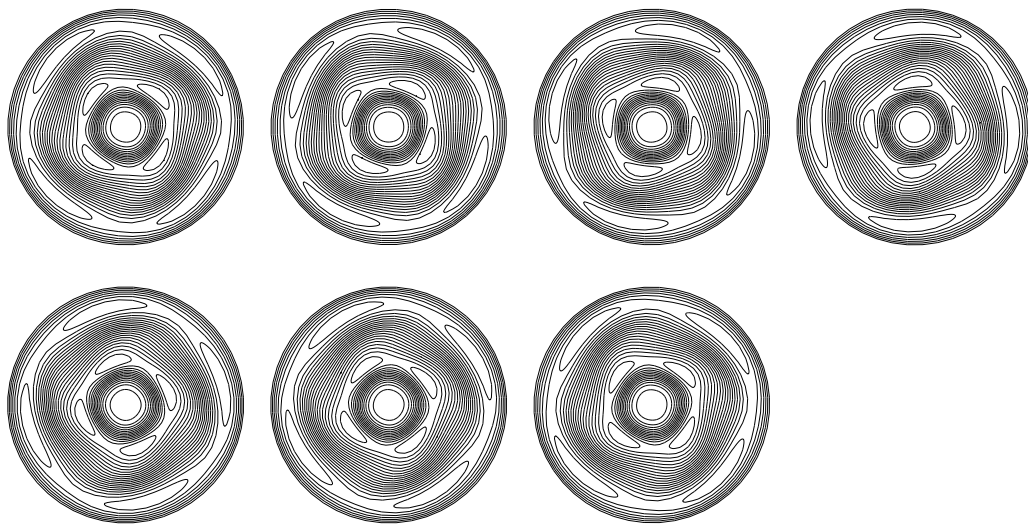


Fig. 13. isolines of the total axial velocity in the plane $z = 0.8A$ for $A = 3$ and $\text{Re} = 2850$; from left to right and up to down: $t = t_0 + iT/6$; $i = 0, \dots, 6$

List of Figures

1	sketch of the configuration	22
2	The MAC grid	22
3	Loops along which the Stokes theorem is applied in order to compute the (a) radial component, (b) azimuthal component, (c) axial component of the vorticity	22
4	Loop to compute the axial component $Z_{k+\frac{1}{2}}$ of the vorticity at a point on the axis $r = 0$ and in the plane $z = (k + \frac{1}{2})\Delta z$	23
5	streamlines for the circular lid driven cavity at $Re = 400$; (a) $\theta_0 = 0$ (b) $\theta_0 = 32$ degrees	23
6	time evolution of the normalized kinetic energy E'/E_0 of the $m = 2$ Fourier mode for $A = 1$ and different values of the Reynolds number	24
7	time evolution of the normalized kinetic energy E'/E_0 of different Fourier modes for $A = 1$ and Reynolds number = 2550	24
8	critical linear threshold as computed for three different grids: $101 \times 32 \times 101$, $161 \times 32 \times 161$, $201 \times 32 \times 201$ in (r, θ, z) and extrapolated to zero	24
9	Time evolution of the kinetic energy of Fourier modes $m = 0$ to $m = 10$ for $Re = 2850$; $A = 3$	24
10	isolines of the axial velocity in the plane $z = 0.8A$; left: fluctuating axial velocity ; right: total axial velocity	25
11	iso-lines of w in meridional planes for azimuthal locations as indicated. The dashed lines are for negative values of w	25
12	Time evolution of the total axial component w of the velocity at two different points. The + symbols correspond to the different patterns of the next figure	25
13	isolines of the total axial velocity in the plane $z = 0.8A$ for $A = 3$ and $Re = 2850$; from left to right and up to down: $t = t_0 + iT/6$; $i = 0, \dots, 6$	26

References

- [1] SOTIROPOULOS AND VENTIKOS, "The three dimensional structure of confined swirling flows with vortex breakdown", *J. Fluid Mech.*, **426**, pp 155–175, 2001
- [2] Y. MADAY AND C. BERNARDI, *Approximations spectrales de problèmes aux limites elliptiques*, Mathématiques et Applications **10**, SMAI, Springer–Verlag, (1992).
- [3] S. XIN, P. LE QUÉRÉ, AND O. DAUBE, " Natural convection in a differentially heated horizontal cylinder: Effects of Prandtl number on flow structure and instability" , *Phys. Fluids*, vol. 9, 1014-1033, (1997).
- [4] R. VERZICCO AND P. ORLANDI, "A finite difference scheme for three dimensional flows in cylindrical coordinates", *J. Comp. Phys.*, **123**,402-414, (1996).
- [5] J.M. HYMAN, M. SHASHKOV, "Natural Discretizations for the divergence, gradient and curl on logically rectangular grids", *Comp. Math. Applic.*, **33** , 81–104, (1997).
- [6] J.M. HYMAN, M. SHASHKOV, "The orthogonal decomposition theorems for mimetic finite difference operators", *SIAM J. Num. Anal.*, **36** #3 , 788–818, (1999).
- [7] J.M. HYMAN, M. SHASHKOV, "Adjoint operators for the natural Discretizations of the divergence, gradient and curl on logically rectangular grids", *Applied Num. Math.*, **25** , 413–442, (1997).
- [8] M.P. ESCUDIER, " Observations of the flow produced in a cylindrical container by a rotating endwall", *Experiments in Fluids*, **2**, 189-196, (1984).
- [9] H.J. LUGT, M. ABBOUD, " Axisymmetric vortex breakdown with and without temperature effects in container with a rotating lid", *J. Fluid Mech.*, **179**, 179–200 , (1987).
- [10] O. DAUBE, Numerical simulation of axisymmetric vortex breakdown in a closed cylinder, *Lectures in Applied Math.*, Ed. AMS, **28**, 131–152, (1991).
- [11] J.M. LOPEZ, " Axisymmetric vortex breakdown. Part 1 . Confined swirling flows", *J. Fluid Mech.*, **221**, 533-552, (1990).
- [12] H.M. BLACKBURN, J.M. LOPEZ, "Symmetry breaking of the flow in a cylinder driven by a rotating endwall ", *Phys. Fluids*, **12**, #11, 2698-2701 , (2000).
- [13] F. MARQUÈS, J.M. LOPEZ, "Precessing vortex breakdown mode in an enclosed cylinder flow ", *Phys. Fluids*, **13**, #6, , (2001).
- [14] E. SERRE AND P. BONToux, " Three dimensional swirling flow with a precessing vortex breakdown in a rotor–stator cylinder", *Phys. Fluid* , **13**, 3500–3503, (2001)

- [15] GELFGAT Y.A., BAR-YOSEPH P.Z. & SOLAN A. "Three-dimensional instability of axisymmetric flow in a rotating lid-cylinder enclosure" *J. Fluid Mech.* **438**, 363–377, 2001
- [16] K. GODA, A multistep technique with implicit difference schemes for calculating two- or three-dimensional cavity flows, *J. Comp. Phys.*, **30**, 76-95, (1979).
- [17] V.G. PRIMAK, " Pseudospectral algorithms for Navier–Stokes simulation of turbulent flows in cylindrical geometries with coordinate singularity", *J. Comp. Phys.*, **118**, 366-379 , (1995).
- [18] M.D. GUNZBURGER, in *Finite Element Method for Viscous Incompressible flows*, pp 12-13, Academic Press, (1989).
- [19] S. A. ORSZAG, " Spectral Methods for Problems in Complex geometries", *J. Comp. Phys.*, **37** # 1 , pp 70-92 , (1980)
- [20] D.B. Haidvogel and T. Zang, "The accurate solution of Poisson's equation by expansions in Chebychev polynomials" ,*J. Comp. Phys.*, **30**, pp. 167–180, 1979
- [21] O. DAUBE, P. LE QUÉRÉ, "Numerical investigation of the first bifurcation in a rotor-stator cavity of radial aspect ratio 10", *Comp. & Fluids*, **31**, pp 481–494 , 2002
- [22] L.S. Tuckerman, Steady-state solving via Stokes preconditioning: Recurrence relations for elliptic operators, *Lecture notes in Physics*, p. 573, edited by D.L. Dwoyer, M.Y. Hussaini, and R.G. Voigt, Springer, New York, 1989.
- [23] E. KNOBLOCH, "Bifurcations in rotating systems", In *Lectures in solar and planetary dynamos*, ed. M.R. Proctor & A.D. Gilbert, pp 331–372, Cambridge University Press, 1994